DESIGN AND FABRICATION OF A VORTEX INERTIAL SENSOR CONSISTING OF 3-DOF GYROSCOPE AND 3-DOF ACCELEROMETER

Zhongjian Xie[1], Honglong Chang[1], Yong Yang[1], Xiaoqing Li[1], Pingwei Zhou[1], and Weizheng Yuan[1]
[1]Northwestern Polytechnical University - MEMS Lab, Xi'an, China

ABSTRACT

This paper reports a novel vortex multi-axis inertial sensor, which can detect three components of angular rate and three components of linear acceleration simultaneously. It uses a vortex gas flow instead of the traditional linear gas flow as the inertial mass to detect the angular rate and linear acceleration. In the implementation, the vortex was formed by jetting the gas into a round chamber through two opposing nozzle orifices in the opposite direction. And the multi-axis detection was realized by a proper configuration of thermistors. The test results show that both the gyroscopes and accelerometers can reach a medium accuracy, which proves the feasibility of the device.

KEYWORDS:

Vortex inertial sensor, thermal convective, 3-axis gyroscope, 3-axis accelerometer, thermistor.

INTRODUCTION

Various MEMS inertial sensors such as gyroscopes and accelerometers have been fully researched in the recent twenty years. Reducing size and cost of inertial sensors has been the focus of the field. Multi-axis inertial sensor allows the minimum size and cost, thus it attracts much attention and some exciting results have emerged. V. T. Dau presented a 5-axis fluidic inertial sensor at transducers 2009 [1]. It used gas flow and thermistor to sense the angular rates or accelerations. M. Kraft presented a latest 5-axis mechanical inertial sensor using a rotating mechanically unconstrained proof mass at IEEE Sensors 2010 [2]. It uses the electrostatic force to levitate the spinning disk and the capacitive sensing technique to detect the angular rates or accelerations. However, it is very difficult to levitate, rotate and control such a rigid proof mass using current technologies.

Compared with the two 5-axis inertial sensors, a new 6-axis inertial sensor based on a vortex proof mass is presented in this paper. It combines the advantages of the fluidic inertial sensor and the mechanical spinning disk sensor together. It uses a vortex proof mass which rotates like the rigid rotor. Compared with the rigid rotor, the vortex is easy to be implemented and can endure high shock resistance. Meanwhile, it is different from the 5-axis fluidic inertial sensor where the linear convection flow [1，3, 4] is used and the multi-axis sensing is realized by forming a fluidic network including four perpendicular flow channels and a pump chamber at the center. In this paper, we demonstrated how to design, fabricate and test such a vortex initial sensor.

WORKING PRINCIPLE

The schematic view of the vortex sensor is shown in Figure 1. It is composed of two nozzle orifices, a detection chamber, double detection layers and two outlets. Thermistors are distributed on detection layer. When it works, gas flow is jetted into the detection chamber through the two nozzles to form a vortex. In the case of an angular rate or a linear acceleration, the vortex would deflect or offset due to its inertia, which can be sensed through thermistor heated by a constant current.

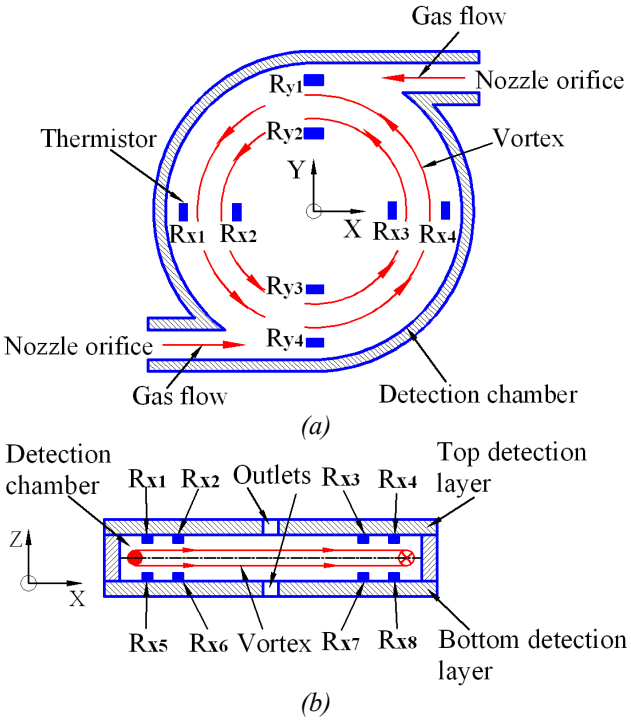

Figure 1: A schematic view of the vortex sensor. (a) Principle of vortex formation of the sensor. (b) Front view of the vortex sensor.

First, the working principle of detecting an angular rate input is shown in Figure 2. Figure 2(a) is the vortex deflection in the case of a Z-axis angular rate. The vortex shrinks from vortex 1 to vortex 2 subjecting to inward Coriolis force. Then differential cooling effects will appear between two thermistors along radial direction. As a result, the resistances of two thermistors will reversely change due to the thermo-resistive effect. Resistance change $\triangle R_{\omega z}$ is calculated by

$$\Delta R_{\omega z} = (R_{x1} + R_{x4} + R_{y1} + R_{y4}) - (R_{x2} + R_{x3} + R_{y2} + R_{y3}) \quad (1)$$

Figure 2(b) is the deflection of vortex in the case of X-axis angular rate. Compared with Figure 1(b), we can find the vortex deflects around Y-axis. Then the resistance change $\triangle R_{\omega x}$ is calculated by

$$\Delta R_{\omega x} = (R_{x2} - R_{x3}) + (R_{x7} - R_{x6}) \quad (2)$$

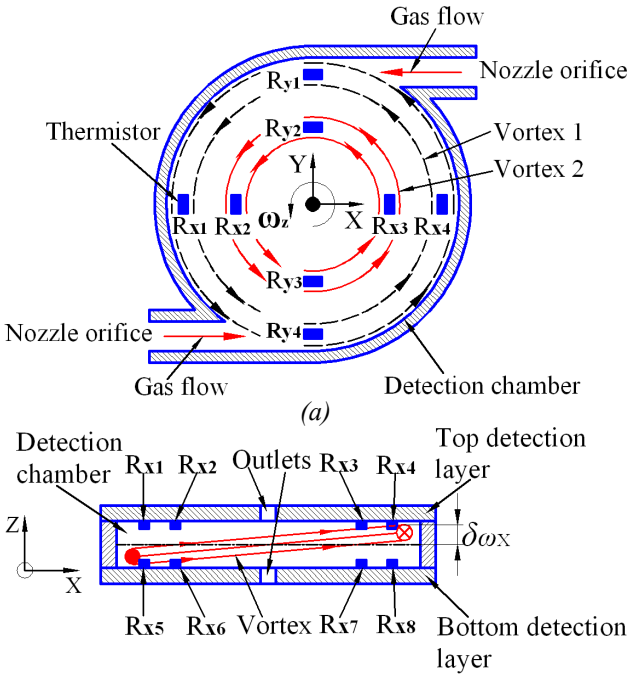

Figure 2: (a) Top view of vortex deflection in the case of an angular rate ω_z due to Coriolis force. (b) Front view of vortex deflection in the case of an angular rate ω_x due to gyroscopic precession.

The detection principle of Y-axis angular rate is the same as X-axis angular rate. As a result, these resistance changes are converted to output voltage by a common Wheatstone bridge.

The vortex gas flow is launched with an initial velocity that is denoted by ω_v. As an angular rate ω is applied, the vortex deflects (Figure 2(b)) due to the Coriolis acceleration a_ω according to

$$a_\omega = 2\omega \times \omega_v \tag{3}$$

The flow velocity of the vortex in deflected direction (the direction of Coriolis acceleration) V_ω is calculated by

$$V_\omega = \int a_\omega dt = \int 2\omega \times \omega_v dt \tag{4}$$

For small deflections and $\omega_v \approx$const, the velocities of the vortex in the deflected directions at the plane of the thermistors are approximately

$$V_{\omega x} = 2\omega_x \cdot \omega_v \cdot t_\alpha \qquad V_{\omega y} = 2\omega_y \cdot \omega_v \cdot t_\alpha$$
$$V_{\omega z} = 2\omega_z \cdot \omega_v \cdot t_\alpha \tag{5}$$

Where t_α is the time that is required for the gas flow to travel from the nozzle orifice to the sensing element. Time t_α can be expressed as the ratio of angle α (from the nozzle orifice to the sensing element) and the flow velocity, i.e., $t_\alpha = \alpha/\omega_v$.

The flow deflection δ_ω is given by further integration with respect to t of V_ω in (4) as

$$\delta_\omega = \int V_\omega dt = \iint 2\omega \times \omega_v dt \tag{6}$$

The three components of vortex deflection in the three sensing directions can be expressed as

$$\delta_{\omega x} = \omega_x \frac{\alpha^2}{\omega_v} \quad \delta_{\omega y} = \omega_y \frac{\alpha^2}{\omega_v} \quad \delta_{\omega z} = \omega_z \frac{\alpha^2}{\omega_v} \tag{7}$$

The deflection $\delta_{\omega x}$, $\delta_{\omega y}$ and $\delta_{\omega z}$ directly affect the sensitivity of the vortex gyroscope, respectively. A larger deflection causes greater difference in the temperatures of the two opposing thermistors; therefore, the output voltage is higher. Equation (7) suggests that gas deflection is directly proportional to the magnitude of the input angular rate. This equation also indicates that the sensitivity depends on the angle α from the nozzle orifice to the sensing element and on rotating speed ω_v of the vortex.

Second, the working principle of detecting linear acceleration is shown in Figure 3. Figure 3(a) is the front view of vortex offset in the case of X-axis linear acceleration. Then differential cooling effects will appear between the thermistors in one side of the detection cavity and the other side's thermistors. Resistance change $\triangle R_{ax}$ is calculated by

$$\Delta R_{ax} = (R_{x2} + R_{x6}) - (R_{x3} + R_{x7}) \tag{8}$$

The detection to the Y-axis linear acceleration is the same as X-axis's detection. Figure 3(b) is the front view of vortex offset in the case of Z-axis linear acceleration. Resistance change $\triangle R_{az}$ is calculated by

$$\Delta R_{az} = (R_{x6} + R_{x7}) - (R_{x2} + R_{x3}) \tag{9}$$

Finally, these resistance changes are converted to output voltage by Wheatstone bridge.

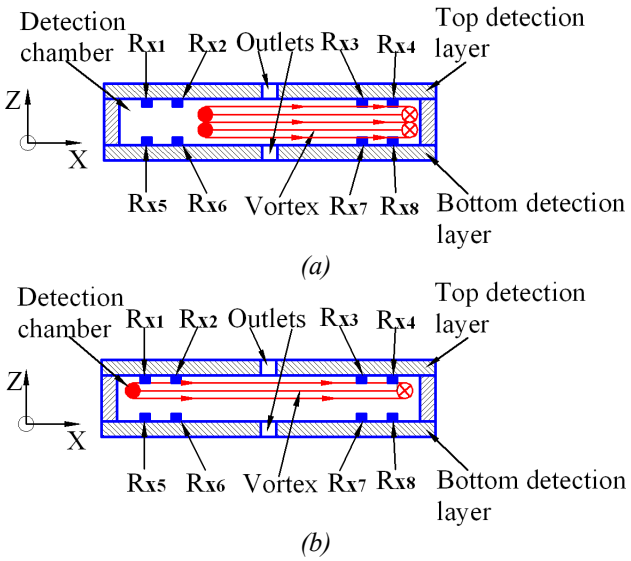

Figure 3: (a) Front view of vortex offset in the case of X-axis linear acceleration. (b) Front view of vortex offset in the case of Z-axis linear acceleration.

The ANSYS-CFX software was employed to simulate motion of the gas flow. Figure 4 shows the vortex pattern inside the detection cavity. It is clear that a vortex is formed. The distribution of flow velocity in the radial direction at the sensing plane is shown in Figure 5. The linear motion region of flow velocity is 1-6 mm from chamber center in the radial direction, which should be chosen as the location of thermistor.

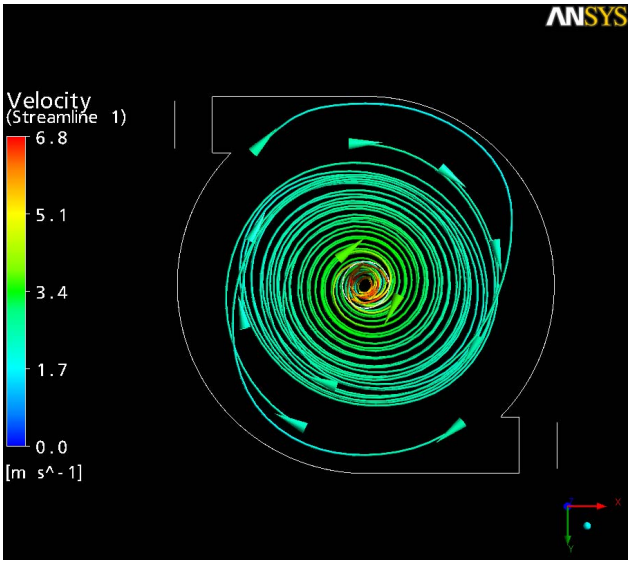

Figure 4: Flow pattern inside detection chamber-vortex.

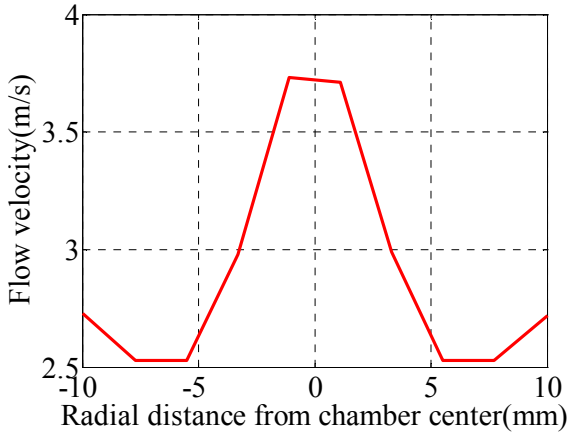

Figure 5: Distribution of flow velocity in radial direction of detection chamber.

FABRICATION AND ASSEMBLY

The thermistor is made of P-type silicon. Figure 6 is structure of the thermistor, which is composed of aluminum pads and silicon sensing element.

The fabrication of the sensing element begins with a silicon-on-insulator (SOI) wafer with a 50-μm-thick p-type device layer and a resistivity of 0.8 Ω•cm (Figure 7(a)). Next, 0.1-μm-thick SiO_2 is grown by thermal oxidization to create the insulating layer. The contact holes are opened through SiO_2 etching (Figure 7(b)). P+ diffusion is performed, and then the oxide is etched by buffered oxide etch (BOE) (Figure 7(c)). Aluminum (Al) anchors of 0.8-μm thickness for interconnection are made by sputtering, photolithography, and Al etching. Then, sintering is carried out to make ohmic contact between the Al anchors and the device layer through the contact holes (Figure 7(d)). The structure of the thermistor is then formed by using inductively coupled plasma deep reactive ion etching (ICP-DRIE) (Figure 7(e)).

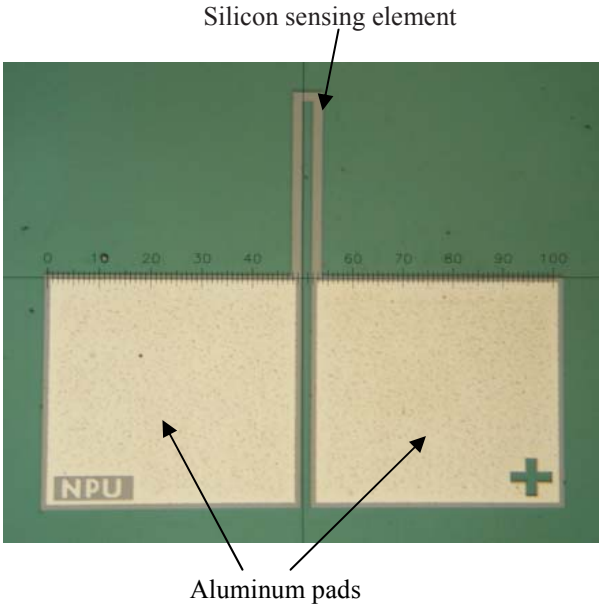

Figure 6: Structure of the thermistor.

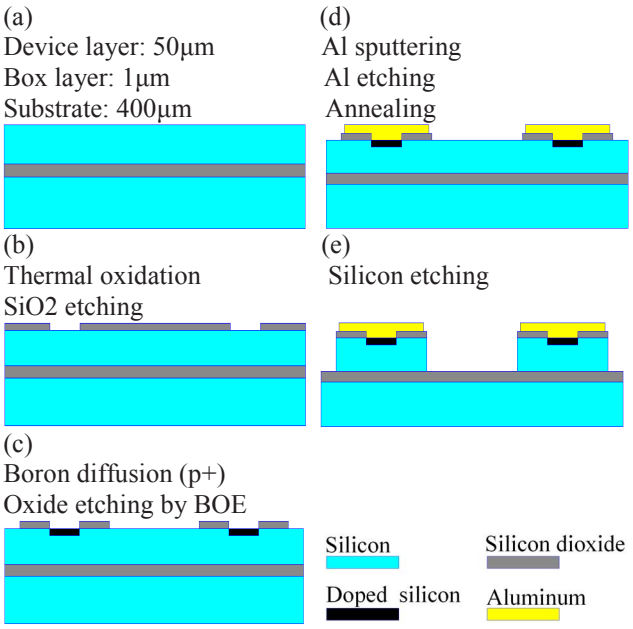

Figure 7: Fabrication process of the sensing element.

Thermistors are glued on PCB board, and then the anchors of thermistors are connected with anchors on PCB board through gold wires. This is called detection board.

The detection chamber is fabricated by conventional machining on Polymethyl methacrylate (PMMA) material with a diameter of 20 mm. Then it is assembled with the detection board.

The entire vortex sensor (Figure 8(a)) is composed of nozzle orifice, detection chamber, outlet, bottom detection board and top detection board. From the cutaway view of the vortex sensor (Figure 8(b)), we can see the location of thermistors in detection chamber.

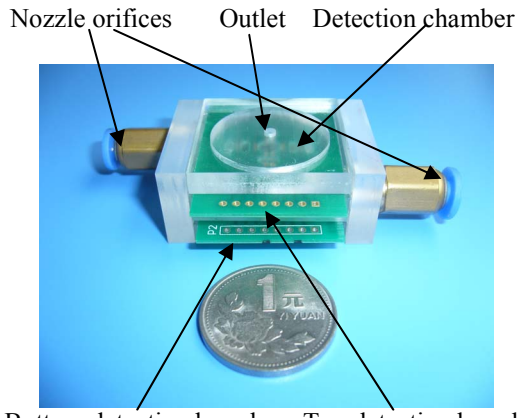

(a)

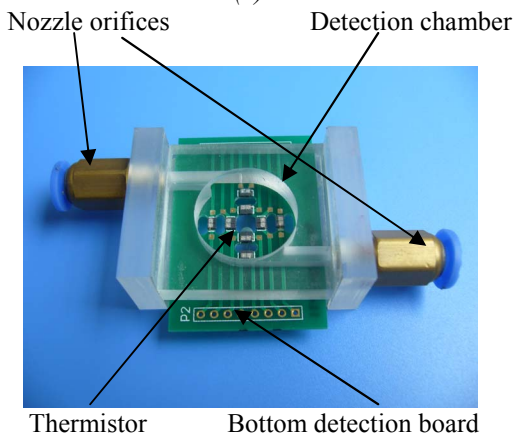

(b)

Figure 8: (a) A schematic view of assembled structure of the vortex sensor with double detection layer. (b) Cutaway view of the vortex sensor with single detection layer.

EXPERIMENTS

The gas flow was supplied by an air pump (Taiwan Honlite). The velocity of the gas flow jetted through the nozzle orifice was measured to be about 5 m/s. The resistance and TCR of the thermistor were measured to be 3.2 kΩ and 4300 ppm/^{o}C, respectively.

As shown in Figure 9, the measured sensitivities of the vortex sensor around X-axis, Y-axis and Z-axis were 0.429 mv/^{o}/s, 0.338 mv/^{o}/s and 0.159 mv/^{o}/s respectively and the nonlinearity for the X-axis, Y-axis and Z-axis were 1.7%, 6% and 4.8% in the range of ±100 ^{o}/s respectively. The measured sensitivities of the linear acceleration for X-axis, Y-axis and Z-axis were 0.185 v/g, 0.180 v/g and 0.133 v/g.

CONSLUSION

Through integrating the MEMS fabrication process with the conventional machining, the first vortex inertial sensor has been achieved in this paper. By testing, the principle of the vortex inertial sensor has been verified preliminarily.

The vortex inertial sensor can realize a six-freedom detection, endure high shock resistance and easy to be implemented. So, it is a promising candidate of multi-axis inertial sensor. In the future, a miniature vortex inertial sensor including the pump can be fully implemented in MEMS process.

ACKNOWLEDGMENT

The authors gratefully acknowledge Chinese National Science Foundation's financial support (No. 60976087) and the support from Chinese New Century Excellent Talents in University (NCET).

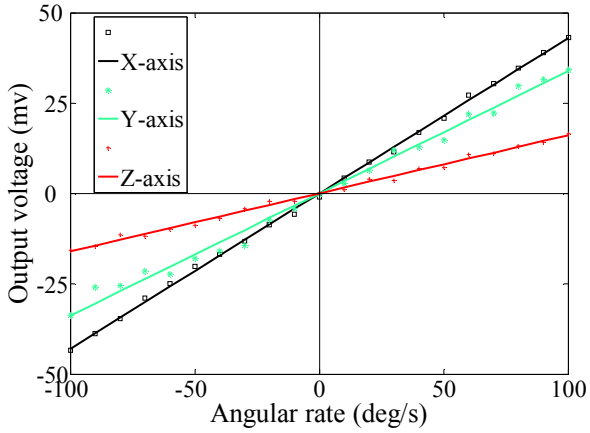

(a)

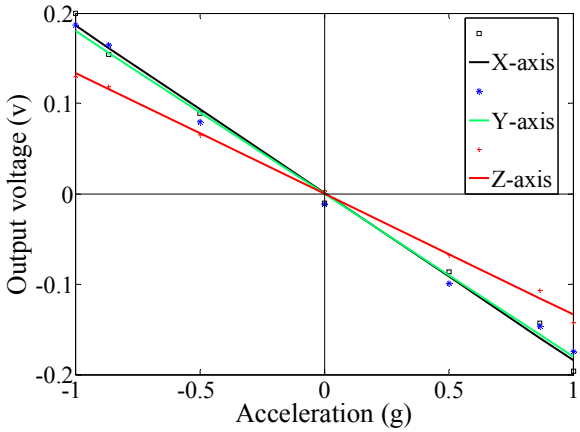

(b)

Figure 9: (a) Output voltage of the vortex sensor versus the applied angular rates. (b) Output voltage of the vortex sensor versus the applied accelerations.

REFERENCES

[1] V. T. Dau, T. Otake, T. X. Dinh and S. Sugiyama, "Design and Fabrication of Convective Inertial Sensor Consisting of 3DOF Gyroscope and 2DOF Accelerometer", *Transducers 2009*, pp. 1170-1173.

[2] M. Kraft and B. Damrongsak, "Micromachined Gyroscopes Based on a Rotating Mechanically Unconstrained Proof Mass", *IEEE SENSORS 2010*, pp. 23-28.

[3] V. T. Dau, O. Tomonori, T. X. Dinh, D. V. Dao and S. Sugiyama, "A Multi Axis Fluidic Inertial Sensor", *IEEE SENSORS 2008*, pp. 666-669.

[4] V. T. Dau, T. X. Dinh and D. V. Dao, "Design and Simulation of Convective Inertial Sensor", *Micro-NanoMechatronics and Human Science, 2008*, pp. 33-36.

CONTACT

Honglong Chang, tel: +86-029-8849-2841;
changhl@nwpu.edu.cn